Check for updates

Advanced Intelligent Discovery

WILEY VCH

ADVANCED INTELLIGENT DISCOVERY Open Access

RESEARCH ARTICLE OPEN ACCESS

Machine Learning-Assisted Infectious Disease Detection in Low-Income Areas: Toward Rapid Triage of Dengue and Zika Virus Using Open-Source Hardware

Marina Ribeiro Batistuti Sawazaki[1] | Bassam Bachour Junior[2] | Marcelo Mulato[2] | José Ilton de Oliveira Filho[3]

[1]Department of Morphology and Animal Physiology, Faculty of Agricultural and Veterinary Sciences, São Paulo State University, Jaboticabal, Brazil | [2]Department of Physics, Faculty of Philosophy, Sciences and Letters at Ribeirão Preto, University of São Paulo, Ribeirão Preto, Brazil | [3]Computer, Electrical, and Mathematical Sciences and Engineering Division (CEMSE), King Abdullah University of Science and Technology (KAUST), Thuwal, Saudi Arabia

Correspondence: José Ilton de Oliveira Filho (jose.deoliveirafilho@kaust.edu.sa)

Received: 15 March 2025 | **Revised:** 26 May 2025 | **Accepted:** 28 May 2025

Funding: Coordenação de Aperfeiçoamento de Pessoal de Nível Superior (CAPES), Grant/Award Number: Finance Code 001; Brazilian Council for Scientific and Technological Development (CNPq), Grant/Award Number: 151658/2022−6

Keywords: dengue | electrochemical sensors | internet of medical things | IoMT | machine learning | tinyML | zika

ABSTRACT

Neglected tropical diseases represent a significant global health problem disproportionately affecting impoverished regions with resource-limited sources. These diseases include mainly dengue, zika, and similar arbovirus infections. Rapid, accurate, and low-cost diagnoses are crucial for effective disease management and control, improving live quality. However, conventional diagnostic methods often face logistical challenges, high costs, and complex infrastructure requirements. As an alternative, point-of-care technologies have emerged for diagnostics in remote and vulnerable areas. Even then, similar biomarkers are difficult to distinguish, compromising the diagnosis. This study shows an affordable platform for dengue and zika detection based on fluorine-doped tin oxide thin films modified with gold nanoparticles and functionalized with DNA aptamers. Nonstructural protein 1 (NS1) proteins from dengue and zika were used as biomarkers. Electrochemical impedance spectroscopy was used to verify aptasensor performance and a custom machine learning model was implemented to distinguish both NS1 protein samples when tested individually and mixed in different proportions. Further the use of low-cost and open-source hardware for the implementation of this model for simultaneous detection, and the limitation of the associated hardware, is discussed. The results show an overall accuracy of 95.3% and a maximum RAM usage of 9.4 kB, enabling its use in low-cost hardware-limited devices (<25 USD).

1 | Introduction

Dengue (DENV) and zika viruses (ZIKVs) are considered a significant global health threat by the World Health Organization (WHO), with particular effects on low-income populations in tropical and subtropical regions in the globe [1]. Predominantly vector borne, these arboviruses are primarily transmitted via the bite of infected Aedes mosquitoes, resulting in frequent outbreaks that place a strain on already vulnerable healthcare systems. Just for dengue cases, more than 390 million people are affected every year globally [2], contributing to a considerable burden with illnesses, including severe types such as dengue hemorrhagic fever that can lead to death without appropriate and timely management [3, 4]. Similarly, ZIKV has led to significant epidemics, with noteworthy focus in the Latin American region, where it causes severe complications such as congenital microcephaly and Guillain–Barré syndrome, further intensifying public health concerns [5, 6]. The socioeconomic impact of these viruses is

This is an open access article under the terms of the Creative Commons Attribution License, which permits use, distribution and reproduction in any medium, provided the original work is properly cited.

© 2025 The Author(s). *Advanced Intelligent Discovery* published by Wiley-VCH GmbH.

profound, leading to considerable healthcare expenditures, productivity losses, and developmental challenges in affected regions [2, 5, 7].

The simultaneous detection of dengue and zika infections poses significant diagnostic challenges due to overlapping clinical symptoms such as fever, rash, joint pain, and headache, which complicate accurate clinical differentiation [8, 9]. The situation is exacerbated by inadequate laboratory infrastructure and limited diagnostic resources prevalent in low-income areas [9]. Additionally, the antigenic similarities between DENV and ZIKV often result in serological cross-reactivity, complicating differential diagnosis and accurate clinical management [8–12].

After infection, the cells produce different structural and nonstructural proteins. Nonstructural protein 1 (NS1) has been extensively used as a biomarker as it is the only protein secreted into blood plasma and can be easily obtained [13]. However, NS1 from both infections has similar structures and can be recognized by the same bioreceptors, making it difficult to distinguish, identify the disease, and follow with the correct treatment [9].

Conventional diagnostic methods, such as polymerase chain reaction (PCR), serological tests like enzyme-linked immunosorbent assay (ELISA), and virus isolation techniques, remain the gold standard but are hindered by the necessity of sophisticated equipment, specialized laboratory conditions, highly trained personnel, and significant turnaround times [8]. These limitations severely constrain their deployment in resource-limited and outbreak-prone areas, limiting timely intervention strategies critical for disease control and management [14, 15].

Artificial intelligence (AI) and machine learning (ML) approaches have emerged as powerful tools to address these diagnostic limitations, offering innovative solutions for enhanced detection efficiency [16–18]. Studies utilizing AI to develop miniaturized diagnostic platforms have demonstrated that the use of ML can significantly improve speed, accuracy, and affordability [19]. These AI algorithms have also been shown to improve biomarker selectivity, even in complex biological fluids [20]. While traditional simultaneous detection of dengue and zika has been demonstrated using modified PCR methods [21, 22], the ML approach has garnered attention for its use in accurate diagnosis during cross-reaction and coinfection [23]. Notably, Zeba et al. demonstrated the use of Logistic regression, support vector machines, random forest, and decision tree models for distinguishing both infectious diseases using a single-cell RNA sequencing dataset (GSE110496) [24]. In their work, a maximum accuracy of 89.4% and a precision of 90% were obtained. While noteworthy accuracy was achieved by traditional ML methods, Sharifrazi et al. demonstrated even higher accuracy, surpassing 95% by combining an ML approach with preprocessing stages [17]. In their approach, multiple ML algorithms were compared, namely CNN, MLP, XGBoost, AdaBoost, random forest, decision tree, naive Bayesian, and logistic regression, yielding an average of 95.3% in accuracy [17]. Furthermore, Arrubla-Hoyos et al. demonstrated the detection and classification using nonbiological data combined with laboratory results. Using random forest technique, they demonstrated 99.1% and 98.8% accuracy for dengue and zika, respectively.

In this study, we propose a novel diagnostic method integrating ML techniques for the simultaneous and rapid triage of dengue and zika infection at the point of testing. Our approach, a fluorine-doped tin oxide (FTO) glass was modified with gold nanoparticles (AuNPs) and functionalized with DNA aptamer to form a self-assembled monolayer (SAM). Electrochemical impedance spectroscopy (EIS) was used to quantify the surface impedance through dengue and zika NS1 proteins interactions. Additionally, the platform was exposed to a mix with different NS1 proportions from the two samples and an ML model was used to distinguish them. We further discuss the implementation of this solution in low-cost settings, using widely available and cheap open-source hardware.

2 | Results and Discussion

2.1 | DENV and ZIKV Sensor Development

FTO was used as a conductive substrate for aptasensor development due to electrical properties suitable for sensitivity, performance requirement, and, at the same, its cost-effectiveness. Substrate surface was activated to obtain hydroxyl groups (—OH) that interacts with 3-(aminopropyl) triethoxylane (APTES), an organosilane molecule used to functionalize oxide surfaces and interacts with AuNPs. AuNPs coated with polyvinyl alcohol (PVA) form stable colloidal structures, prevent aggregation, and promote a uniform and stable thin film over the electrode surface, thereby modifying it (Figure 1a).

For functionalization, aptamer sequences with thiol group and 6-mercapto-1-hexanol (MCH) interacts spontaneously with AuNPs, creating an SAM, and blocked with bovine serum albumin (BSA) to prevent nonspecific interactions. The aptasensor platform was tested with different NS1 concentration from only dengue and zika individually (Figure 1b). Then, the proportions for dengue:zika were tested: 10:90, 20:80, 30:70, 40:60, and 50:50, as percentages.

Figure 2a presents the Nyquist diagram for this aptasensor platform (■) without NS1 interaction obtained from EIS. Target protein was diluted on PBS and each concentration interacted 30 min with the biosensor surface, from 0.01 ng mL^{-1} (●) to 100 ng mL^{-1} (◀), increasing the surface impedance due to the physically and electrostatic blocking. In this case, the graphic present the data for samples with 50% NS1 from dengue and 50% NS1 from zika (50:50). However, the same electrochemical profile was obtained for the proportions between dengue and zika tested.

All data were fitted using the classical equivalent electrochemical circuit illustrated in Figure 2b, composed of solution resistance, indicated as R_S, and the parallel representing the charge transfer resistance (R_{CT}) and the constant phase element (CPE). For electrochemical analysis, the information obtained only from R_{CT} was statistically analyzed using four individual electrodes.

The biosensor was tested over different target concentrations to verify the linear response, surface saturation, and sensibility to each protein and the mix 50:50, as presented in Figure 2c.

29439981, 2026, 2, Downloaded from https://advanced.onlinelibrary.wiley.com/doi/10.1002/aidi.202500049 by Universidade Estadual Paulista, Wiley Online Library on [28/09/2026]. See the Terms and Conditions (https://onlinelibrary.wiley.com/terms-and-conditions) on Wiley Online Library for rules of use; OA articles are governed by the applicable Creative Commons License

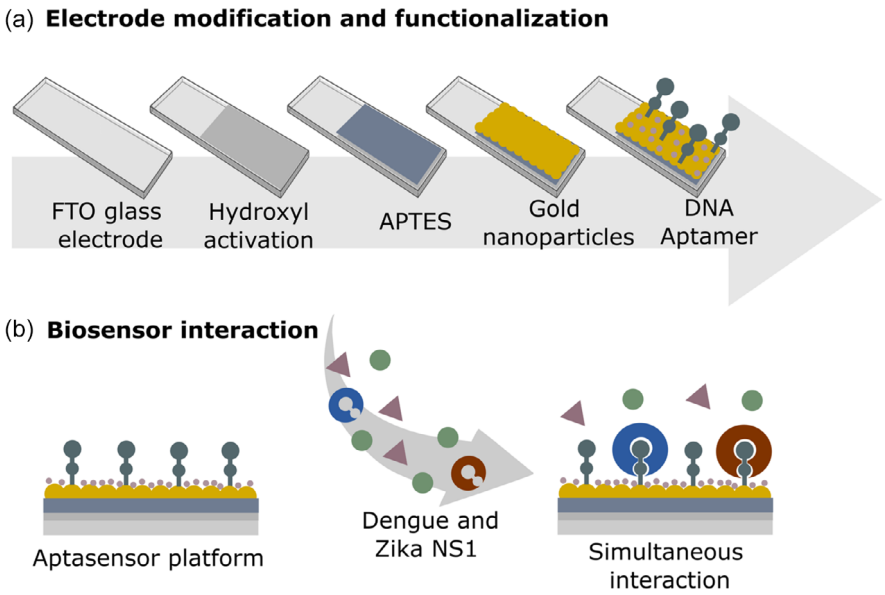


FIGURE 1 | Aptasensor illustration. (a) The steps stated with clean FTO substrates where the surfaces were hydroxylated and modified with APTES and AuNPs, follow by functionalization with DNA aptamers and MCH. (b) Aptasensor platform in ready to interact with NS1 from dengue and from zika, leading to specific interaction on the surface.

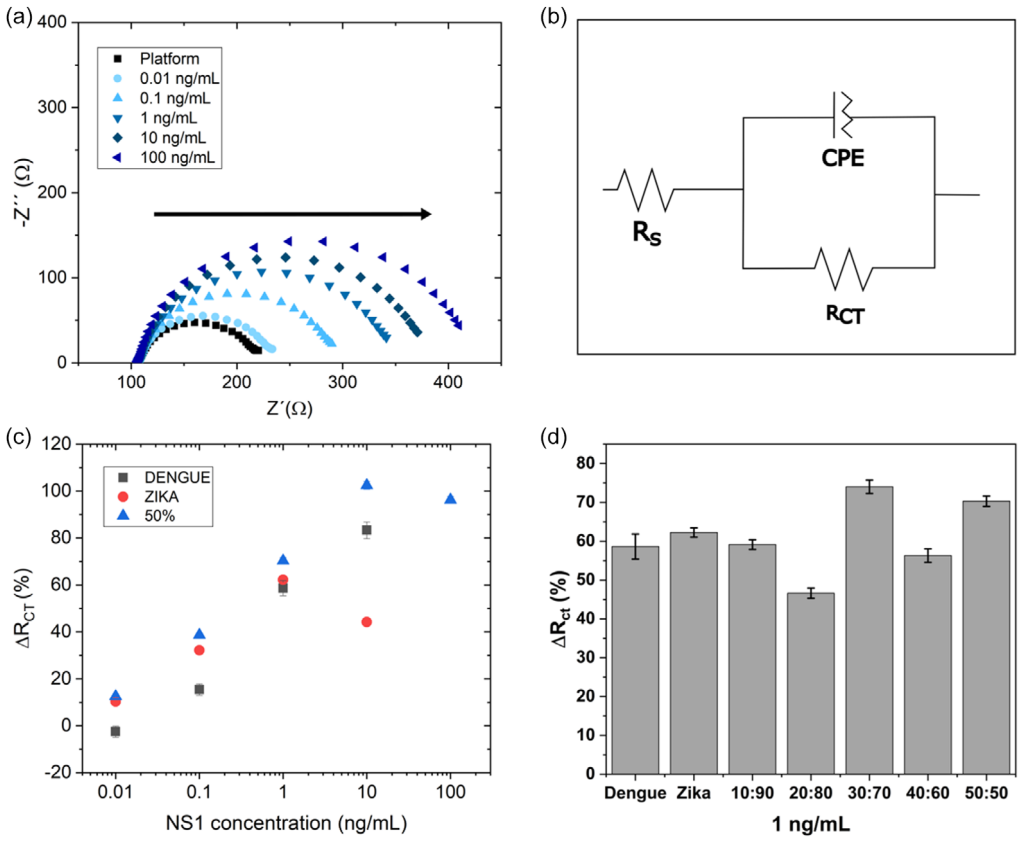


FIGURE 2 | Electrochemical analysis. (a) Nyquist diagram for aptasensor platform and five different NS1 concentrations. (b) Equivalent electrochemical circuit used to fit the impedance data. (c) Change in charge transfer resistance (ΔR_{CT}) for dengue, zika, and 50:50 concentrations. (d) Change in charge transfer resistance (ΔR_{CT}) for 1 ng/mL dengue, zika, and proportions between dengue:zika tested.

From 0.01 to 10 ng mL^{-1}, the platform presented a linear increase and similar behavior, except for dengue 10 ng mL^{-1}, reducing the signal. Surface saturation should occur for 100 ng mL^{-1} or higher. It is possible to observe that the mix with 50:50 of each protein shows a higher response compared with individually samples (Figure 2d), what can be related with the amount of target available on the surface.

Figure 2d presents the 1 ng mL^{-1} result for all proportions where the ΔRCT increased from 45% to 75%, however possible to

29439981, 2026, 2, Downloaded from https://advanced.onlinelibrary.wiley.com/doi/10.1002/aidi.202500049 by Universidade Estadual Paulista, Wiley Online Library on [28/09/2026]. See the Terms and Conditions (https://onlinelibrary.wiley.com/terms-and-conditions) on Wiley Online Library for rules of use; OA articles are governed by the applicable Creative Commons License

observe a relation with the amount of protein from dengue or from zika.

This simple and low-cost approach for dengue and zika detection presented a linear response in from 0.1 to 10 ng mL^{-1} where most of the detection tests works. However, this classical electrochemical signal quantification it is not suitable to distinguish one infection from the other.

2.2 | Embedded ML Model Development

Traditional methods for sensor evaluation using EIS are based on the Nyquist plot results, taking into consideration only the real impedance (Z'/Ω) and imaginary part of impedance ($-Z''/\Omega$), largely ignoring the magnitude (Z/Ω) and phase (°), as it can be derived from the Nyquist. However, in our approach, we utilize the entirety of the data produced in the EIS measurement, as well as preprocessed data from the measurement, improving the final ML classification. The preprocessing and feature extraction steps implemented prior to model training significantly influence the performance and interpretability of the ML approach. In this study, data processing was performed using the Edge Impulse development platform, yielding three data inputs: raw data, flattened data, and spectral data.

The raw data fed directly into the model maintains the original integrity and complexity of the electrochemical impedance measurements but may introduce challenges due to noise and overlapping signal features. Thus, the flattened data provides additional key analytical features allowing more accurate predictions. Nevertheless, both raw and flattened are not enough, as EIS explores the behavior of the sensor response in multiple frequencies, it is also necessary to further process the data, performing spectral analysis using the fast Fourier transform (FFT). This transformation helps to isolate critical frequency-domain characteristics that differentiate analytes, especially valuable when dealing with signals showing similar or overlapping temporal profiles. Spectral features can reduce noise and amplify distinguishing characteristics between closely related electrochemical signals, thus significantly improving classification performance. Collectively, these preprocessing strategies enable the extraction of meaningful features, enhancing the reliability, indispensable for the precise differentiation between analytes such as dengue and zika and their mixtures. Although the combined features as input yields better accuracy, the preprocessing of the data at the edge is limited to floating-point units (float32), FFT serving as one of the main bottlenecks for such. The restriction to 32-bit model limits the use of very low-cost hardware, such as inexpensive (<$1) microcontroller units (MCUs). Further studies on model quantization to an 8-bit should be developed in order to mitigate this issue.

Using a Raspberry Pi (RPI) 5 module as target, the computational burden for the preprocessing is negligible, summing up to 2 KB of RAM and less than 1 ms for preprocessing a single EIS

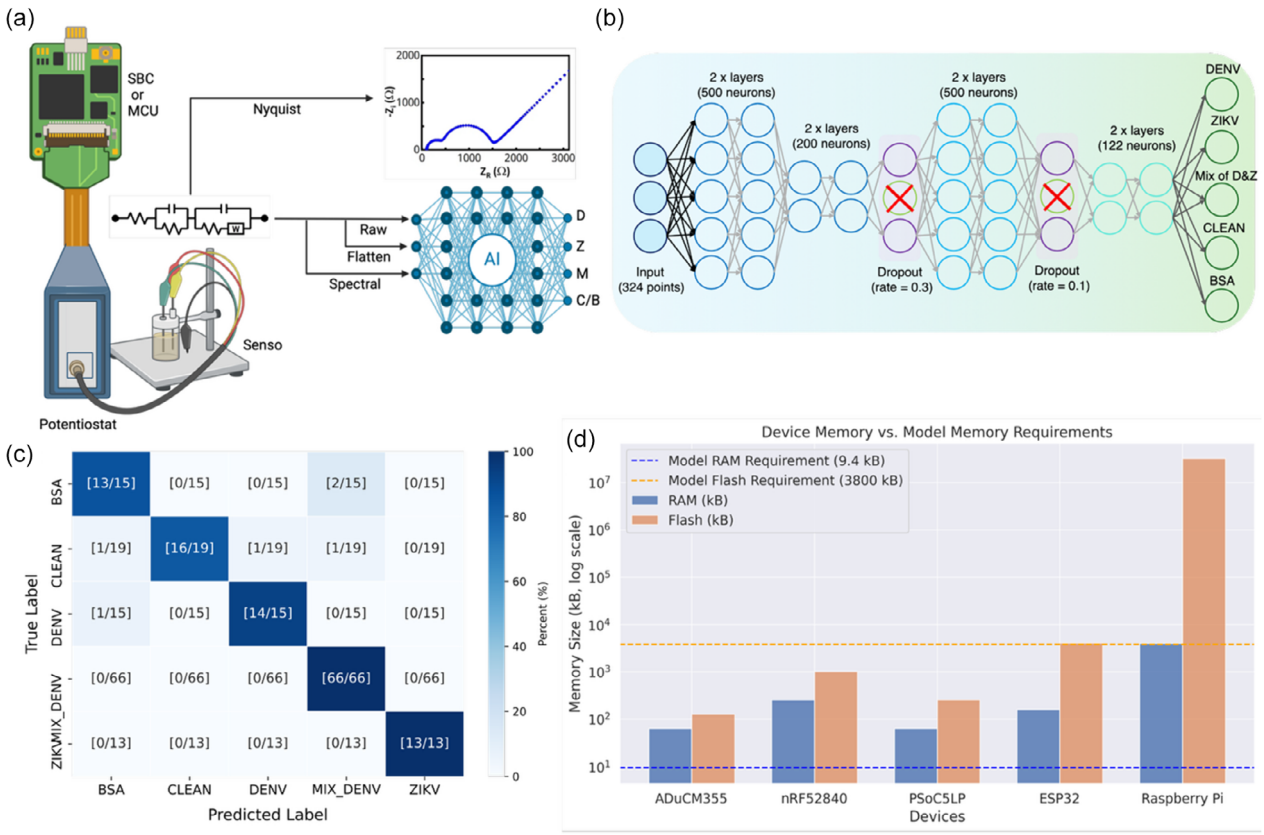


FIGURE 3 | (a) Overview illustration of the rapid triage system for the detection of DENV and ZIKV and its mixtures. (b) ML model architecture. (c) Confusion matrix showing the results of the classification versus the true label. (d) Hardware resources comparison histogram of the mostly used devices for electrochemical readout system in point-of-care application and the model's minimum hardware requirement.

29439981, 2026, 2, Downloaded from https://advanced.onlinelibrary.wiley.com/doi/10.1002/aidi.202500049 by Universidade Estadual Paulista, Wiley Online Library on [28/09/2026]. See the Terms and Conditions (https://onlinelibrary.wiley.com/terms-and-conditions) on Wiley Online Library for rules of use; OA articles are governed by the applicable Creative Commons License

measurement. Nevertheless, the migration of this model for 32-bit supported MCUs typically used for electrochemical measurement, such as ADuCM355 [25, 26], nrf52840 [27], PSoC5LP [28–31], and more widely used ESP32 [20, 32–34], results in a non-negligible RAM usage. Table S1 shows the simulated model results in these MCUs. In the case of ESP32, most demonstrations for electrochemical detection utilize bluetooth low energy (BLE) for data transfer, and once the BLE stack is used, the usable RAM can drop to 16 KB or 32 KB if trace memory is used. Therefore, the preprocessing hardware cost can be up to 12.5% of the RAM for edge applications.

Figure 3b shows the ML model architecture developed in this work. The model works as a classifier for electrochemical signals, inferring on their likelihood of being a sample with single detection of DENV, ZIKV, or a mixture of dengue and zika (MIX_DENVZIKV). Two other classes are added for quality assessment of the sensor before undergoing any sample analyses. These classes are clean sensor (CLEAN) and BSA solution. The addition of these two quality assessment classes is fundamental to address the possible contamination of the sensor, or even to assess whether the sensor is behaving similarly to the ones used in the dataset. Changes in the sensor or even in the electrode may introduce different behavior to the EIS response, leading to a misdetection in a real-world scenario. To avoid this issue, the detection of dengue and zika can only be performed after the quality assessment is done.

The ML results on the validation dataset show an overall accuracy of 95.3% and a low loss of 0.08. Figure 3c shows the ML results from the test set. The results indicate high efficacy in differentiating between the dengue and zika and the mix of both in the same sample. To avoid overfitting in the results, we significantly increased the dataset using real measurements and added two dropout layers with the rate of 0.3 and 01, as shown in Figure 3b. The total dataset was composed of 800 EIS measurements, and each measurement combines four raw time series curves, four processed time series curves, and one flattened sequence. The dropout layer in our model randomly sets a fraction of the neurons (30% and 10%) to zero during each training iteration, effectively preventing neurons from co-adapting too closely to the training data [35, 36].

From the confusion matrix, the model performs with high accuracy (100%) in zika and mixed samples, while in dengue it shows less accuracy (93.3%). Similarly, the BSA and clean category demonstrated classification precision of 86.7% and 84.2%, respectively. The misclassification primarily occurred between the mixed and BSA classes, mostly in the picomolar range spiked samples. The total model requires 3.8 MB of flash memory and 9.4 kB of RAM to operate. Figure 3d shows the histogram of commonly used devices for electrochemical measurements and the required memory footprint.

2.3 | ML Model Deployment in Open-Source Hardware

In order to focus the deployment on low cost settings, we selected RPI 5 and Zero W versions as the target hardware for model deployment. RPI boards are single-board computer modules that

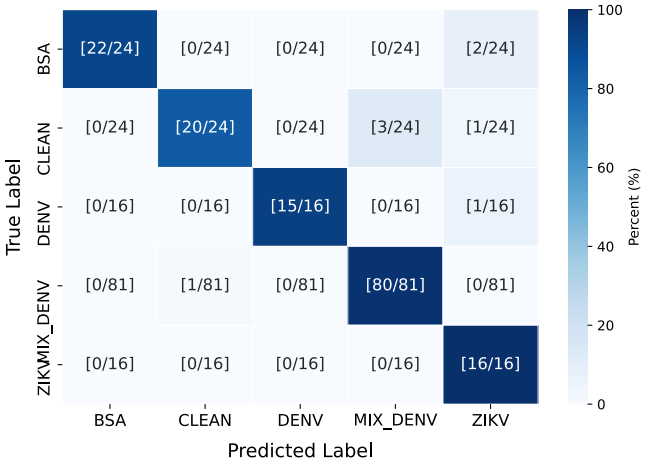


FIGURE 4 | Confusion matrix for unseen data showing the correct predicted percentage for BSA (91.7%), clean (83.3%), DENV (93.8%), ZikV (100%), and mix samples of DENV and ZIKV (98.8%). The diagonal elements of this confusion matrix represent the percentage of correctly classified solutions, while the off-diagonal elements reflect the percentage of misclassified ones. The uncertain column denotes the proportion of instances where the model was unable to classify with confidence above the set threshold.

are widely available around the world, retailing at a cost of ~$15 for RPI W, ~$24 for RPI 2W, and ~$80 for RPI 5. The specs of these modules are detailed in Table S2 in the supplementary.

The model was deployed on the RPI versions, using online and offline methods. The RPI support online deployment using command-line interface (CLI), however, only the RPI 5 and 2W version supports the offline deployment using native Linux binary application. The reason for that is Edge Impulse model (EIM) binaries for Linux can only run on advanced RISC machine v7 (ARMv7) or ARM64, respectively, the 32-bit and 64-bit execution state of the ARM architecture family. While the RPI W uses a Broadcom chip with ARMv6. The ML model was tested using unseen EIS data curves, and results are presented in Figure 4.

For the model implementation, samples of BSA, clean, and dengue showed uncertainty smaller than the defined threshold (90%), with dengue and BSA showing the higher degree of uncertainties, 6.3% and 8.3%, respectively. It is noteworthy that for biological samples, it is desirable to provide uncertainty level in the results and have a high threshold limit for classification. This step helps mitigate misdiagnoses and false negatives [37], a major hurdle of using ML in healthcare.

3 | Conclusion

In conclusion, the sample and low-cost approach for dengue and zika aptasensor show the target–bioreceptor interaction in different concentrations in the clinical range. However, the classical electrochemical analysis considers only the real impedance, and the imaginary part of impedance cannot distinguish dengue from zika or even quantify the amount of target from each infection. Thus, the application of the machine offers a simple-yet efficient solution for rapid detection of both viruses, yielding

29439981, 2026, 2, Downloaded from https://advanced.onlinelibrary.wiley.com/doi/10.1002/aidi.202500049 by Universidade Estadual Paulista, Wiley Online Library on [28/09/2026]. See the Terms and Conditions (https://onlinelibrary.wiley.com/terms-and-conditions) on Wiley Online Library for rules of use; OA articles are governed by the applicable Creative Commons License

an overall accuracy of 95.3%. Furthermore, due to the incidence of both diseases largely in low-income populations, finding a low-cost solution is paramount and essential for the practical adoption of such a solution. However, the high hardware penalty for the data preprocessing limits the application of our model in 32-bit hardware, elevating the final cost of the application. Nevertheless, we demonstrate that it is still possible to implement the model in low-cost hardware under 30 USD. This work opens the possibility for the development of more complete electrochemical systems, in which the triage of both viruses can be done at the edge, directly in the potentiostat device or in the potentiostat interface machine.

4 | Experimental Section

Materials: DNA aptamer sequence 5′ - HS $(CH_2)_6$ – TTTTAGCGGATCCGATGGGTGGG GGGGTGGGTAGGATCC GCG - 3′ was purchased from Exxtend Biotecnologia. Dengue NS1 serotype 4 (NS1-S4) was purchased from Abcam (ab181957). Zika nonstructural protein was purchased from Elabscience (PKSV 030273). FTO thin films deposited on glass; biological pure ethanol; phosphate buffered saline tablet (PBS); MCH; BSA; sodium phosphate dibasic and monobasic (Na_2HPO_4 and KH_2PO_4, respectively); magnesium dichloride ($MgCl_2$); ethylenediaminetetraacetic acid (EDTA); potassium hexacyanoferrate (III) and potassium hexacyanoferrate trihydrate (Il), sodium borohydride (NaBH4), acetone (2-propanone), biological pure ethanol, APTES, and TE (Tris + EDTA) buffer were all purchased from Sigma–Aldrich. Potassium chloride (KCI) was purchased from Cinetica. Sodium chloride (NaCl) and hydrogen peroxide (H_2O_2) were obtained from Synth. Tetrachloroauric acid ($HAuCl_4{\cdot}3H_2O$) was obtained by Exodo Cientifica. PVA—$(C_2H_4O)_x$ and ammonium hydroxide (NH_4OH) were obtained by VETEC. All aqueous solutions were prepared using 18.2 MQ.cm ultrapure water (Merck Millipore Direct-Q 5UV) with a Biopak Polisher filter (Merck Millipore, CDUFB-001) to remove nuclease. All the chemicals were analytical or commercial grade.

Nanoparticle Synthesis: AuNPs were synthesized according to Oliveira [38]. Briefly, 250 µL PVA (0.05 g mL^{-1}) were added to 100 mL borohydride solution (0.30 g mL^{-1}). After that, this solution was added to 100 mL tetrachloroauric acid (0.8 g mL^{-1}) under vigorous stirring and kept overnight. To remove residues, AuNPs colloidal dispersion was dialyzed in Milli-Q for 5 days with daily water replacement.

FTO Cleaning and Modification: FTO glass substrates of size 1×2.5 cm^2 were sonicated with acetone, pure ethanol, and deionized water for 5 min each dried with nitrogen gas. Clean substrates were immersed in hydroxylation solution (H_2O_2 + NH_4OH) diluted in Mili-Q water (1 : 1:5) and dried for 30 min at 60°C. After that, the substrates were immersed in APTES (1%, v/v pure ethanol) solution for 1 h, washed with ethanol, and dried with nitrogen gas. Finally, modified substrates were immersed in AuNP solution for 2 h and dried with nitrogen gas.

Electrode Functionalization: DNA aptamer sequence was purchased on lyophilized form, diluted in TE buffer, aliquoted, and stored in −40°C until use. Each sample was heated 10 min at 94°C in a water bath and kept at room temperature for 1 h. After that, the sample was diluted in immobilization solution (127.6 g mL^{-1} phosphate buffer (PB) + 58.4 g mL^{-1} NaCl + 0.48 $MgCl_2$ + 0.9 g mL^{-1} EDTA, pH 7.0). Modified FTO electrodes were co-immobilized with 100 µl DNA aptamer and MCH solution (10% ethanol) for 16 h in a humidity chamber, at 4ºC to form an SAM. The platform surface was cleaned using three solutions (31.9 g mL^{-1} PB; 1.6 g mL^{-1} PB + 29.2 g mL^{-1} mM EDTA; and 1.6 g mL^{-1} PB) to remove unbounded sequences and backfilled with 100 µl of MCH (10% ethanol) for 1 h. Finally, electrodes were blocked with BSA (0.1%) in PBS and incubated with different NS1 concentration for 30 min each [39], as illustrated in Figure 1.

Electrochemical Measurements: EIS measurements were performed using a potentiostat (Metrohm/Autolab PGSTAT302) with frequency response analyzer (FRA) module in a three-electrode cell configuration: platinum wire (Metrohm) as counter electrode, Ag/AgCl (FACTE) as reference electrode and functionalized electrode as working electrode. All measurements were performed using 0.92 g mL^{-1} of hexacianoferrato (II) and 0.82 g mL^{-1} of hexacianoferrato (III) in PBS buffer, pH 7.4, over the frequency range from 100 kHz to 5 Hz with a 10 mV AC voltage superimposed on a DC bias of open-circuit potential.

Open-Source Hardware Preparation: We utilized two RPI Zero, versions W and 2W. Both RPIs were flashed with the same 32-bit Raspbian OS, which was installed in a 32 GB SD memory card using the RPI Imager software. The RPI 5 was flashed with 64-bit Raspbian OS.

Electrochemical Dataset Generation: To compose the dataset used in this work, we scanned five different concentrations of dengue and zika between 10 pg mL^{-1} and 100 ng mL^{-1}. For each concentration, we scanned five times with three different electrodes (*triplicate*). The electrochemical technique used was EIS, each EIS measurement generates six arrays with a maximum of 61 data points. From these six arrays (index, frequency [Hz], Z′ [Ω], −Z″ [Ω], Z [Ω], −phase [°], time [s]), we utilized four (frequency [Hz], Z′ [Ω], −Z″ [Ω], Z [Ω], −phase [°]) and use them as 244 raw data points input of the ML model, without additional transformations. We applied two preprocessing techniques (flattening and spectral analysis) to generate 80 additional data points, resulting in a total input of 324 points per EIS measurement. For the mix of zika and dengue, we replicate the same concentrations as for the single measurement, but combining the samples with a rate of 10:90, 20:80, 30:70, 40:60, and 50:50. A custom code written in Python to augment the data using four different techniques: jittering, scaling, jittering with scaling, and random scaling at random points. The augmented data was then mixed with unseen samples to create a mixed test set. The augmented samples systematically mimic noise and realistic perturbations that can be observed while deploying our system in low-income areas, creating a better test set for our proposed solution. All the data generated by this work is available as open source in the GitHub repository for further replication and improvement of this work.

Data processing: All the raw values from the EIS are fed into the model as a time series data together with two other arrays from flattening and spectral process. The flattening preprocessing method simplifies the raw data structure by converting the

29439981, 2026, 2, Downloaded from https://advanced.onlinelibrary.wiley.com/doi/10.1002/aidi.202500049 by Universidade Estadual Paulista, Wiley Online Library on [28/09/2026]. See the Terms and Conditions (https://onlinelibrary.wiley.com/terms-and-conditions) on Wiley Online Library for rules of use; OA articles are governed by the applicable Creative Commons License

multidimensional time-series data into a 1D array, suitable for straightforward input into fully connected neural networks. This array is composed by the extraction of each curve's average, minimum, maximum, root–mean square, standard deviation, skewness, and kurtosis. The flattening process results in a 28 data points, that are feed into the model simultaneously with the raw data. The spectral features array is extracted by performing spectral analysis using FFT with a length of 16. The logarithmic scaling and overlapping FFT frames were used to enhance the frequency domain's resolution and the representation of spectral energy. The processing block codes in Python language is available at Data Availability Statement, and a diagram illustrating the process in presented at Figure S1.

ML Model: The model was developed using the Edge Impulse platform, targeting the RPI 5. Data was imported via the CSV wizard, where the dataset was automatically split into 80% for training and 20% for testing. The input data was processed as a time-series with a window size of 61 s. The final model architecture consisted of eight dense layers, incorporating two dropout layers to prevent overfitting. The first dropout layer, positioned after the fourth dense layer, had a dropout rate of 30%, while the second, placed after the sixth layer, had a rate of 10%. Training was conducted on a CPU over 300 cycles with a learning rate of 0.0001. No learning optimizer was applied. The model was then optimized for edge devices using TensorFlow Lite and converted to EIM and accessed online using CLI.

Acknowledgments

This work was supported by Coordenação de Aperfeiçoamento de Pessoal de Nível Superior (CAPES) (Finance Code 001) and by Brazilian Council for Scientific and Technological Development (CNPq) (151658/2022−6).

Conflicts of Interest

The authors declare no conflicts of interest.

Data Availability Statement

The data that support the findings of this study are openly available in [Github] at [https://github.com/joseiltonfilho/DenV_ZikV-ML], reference number [1].

References

1. W. H. Organization, *Laboratory Testing for Zika Virus and Dengue Virus Infections: Interim Guidance* (2022).

2. Y. Liang and X. Dai, "The Global Incidence and Trends of Three Common Flavivirus Infections (Dengue, Yellow Fever, and Zika) from 2011 to 2021," *Frontiers in Microbiology* 15 (2024): 1458166.

3. S. K. Gahlaut, A. Pathak, B. D. Gupta, and J. Singh, "Portable Fiber-Optic SPR Platform for the Detection of NS1-Antigen for Dengue Diagnosis," *Biosensors and Bioelectronics* 196 (2022): 113720.

4. M. G. Guzman, D. J. Gubler, A. Izquierdo, E. Martinez, and S. B. Halstead, "Dengue Infection," *Nature Reviews Disease Primers* 2, no. 1 (2016): 1–25.

5. Z. Guo, W. Jing, J. Liu, and M. Liu, "The Global Trends and Regional Differences in Incidence of Zika Virus Infection and Implications for Zika Virus Infection Prevention," *PLOS Neglected Tropical Diseases* 16, no. 10 (2022): e0010812.

6. L. L. Santos, E. C. de Aquino, S. M. Fernandes, Y. M. F. Ternes, and V. C. d. R. Feres, "Dengue, Chikungunya, and Zika Virus Infections in Latin America and the Caribbean: A Systematic Review," *Revista Panamericana De Salud Publica* 47 (2023): e34.

7. V. Schiariti, E. Longo, and A. C. De Campos, "Impact of Congenital Zika Virus and COVID-19 on Childhood Disability in Latin America," *Developmental Medicine and Child Neurology* 63, no. 11 (2021): 1241.

8. B. D. P. Dias, et al., "Challenges in Direct Detection of Flaviviruses: A Review," *Pathogens* 12, no. 5 (2023): 643.

9. T. M. Sharp, M. Fischer, J. L. Muñoz-Jordán, et al., "Dengue and Zika Virus Diagnostic Testing for Patients with a Clinically Compatible Illness and Risk for Infection with Both Viruses," *MMWR. Recommendations and Reports* 68 (2019): 1–10.

10. M. D. R. Q. Lima, et al., "The Inability of a Dengue NS1 ELISA to Detect Zika Infections," *Scientific Reports* 9, no. 1 (2019): 18596.

11. B. Cracknell Daniels, et al., "Predicting the Infecting Dengue Serotype from Antibody Titre Data Using Machine Learning," *PLOS Computational Biology* 20, no. 12 (2024): e1012188.

12. R. Zargari Marandi, et al., "Development of a Machine Learning Model for Early Prediction of Plasma Leakage in Suspected Dengue Patients," *PLOS Neglected Tropical Diseases* 17, no. 3 (2023): e0010758.

13. J. Sun, S. Du, Z. Zheng, G. Cheng, and X. Jin, "Defeat Dengue and Zika Viruses with a One-Two Punch of Vaccine and Vector Blockade," *Frontiers in Microbiology* 11 (2020): 362.

14. M. S. Santoso, B. Yohan, D. Denis, et al., "Diagnostic Accuracy of 5 different Brands of Dengue Virus Non-Structural Protein 1 (NS1) Antigen Rapid Diagnostic Tests (RDT) in Indonesia," *Diagnostic Microbiology and Infectious Disease* 98, no. 2 (2020): 115116.

15. J. B. S. Junior, E. Massad, A. Lobao-Neto, R. Kastner, L. Oliver, and E. Gallagher, "Epidemiology and Costs of Dengue in Brazil: A Systematic Literature Review," *International Journal of Infectious Diseases* 122 (2022): 521–528.

16. S. Jain, M. Nehra, R. Kumar, et al., "Internet of Medical Things (IoMT)-Integrated Biosensors for Point-of-Care Testing of Infectious Diseases," *Biosensors and Bioelectronics* 179 (2021): 113074.

17. D. Sharifrazi, N. Javed, R. Alizadehsani, P. N. Paradkar, U. R. Acharya, and A. Bhatti, "Automated Detection of Zika and Dengue in Aedes Aegypti Using Neural Spiking Analysis: A Machine Learning Approach," *Biomedical Signal Processing and Control* 96 (2024): 106594.

18. S. W. Oliveira, L. Cardoso-Sousa, R. P. Georjutti, et al., "Salivary Detection of Zika Virus Infection Using ATR-FTIR Spectroscopy Coupled with Machine Learning Algorithms and Univariate Analysis: A Proof-of-Concept Animal Study," *Diagnostics* 13, no. 8 (2023): 1443.

19. F. Cui, Y. Yue, Y. Zhang, Z. Zhang, and H. S. Zhou, "Advancing Biosensors with Machine Learning," *ACS Sensors* 5, no. 11 (2020): 3346–3364.

20. J. I. de Oliveira Filho, M. C. Faleiros, D. C. Ferreira, V. Mani, and K. N. Salama, "Empowering Electrochemical Biosensors with AI: Overcoming Interference for Precise Dopamine Detection in Complex Samples," *Advanced Intelligent Systems* 5, no. 10 (2023): 2300227.

21. J. A. Boga, M. E. Alvarez-Arguelles, S. Rojo-Alba, M. Rodríguez, M. de Oña, and S. Melón, "Simultaneous Detection of Dengue Virus, Chikungunya Virus, Zika Virus, Yellow Fever Virus and West Nile Virus," *Journal of Virological Methods* 268 (2019): 53–55.

22. D. A. Álvarez-Díaz, E. Valencia-Álvarez, J. A. Rivera, et al., "An Updated RT-qPCR Assay for the Simultaneous Detection and Quantification of Chikungunya, Dengue and Zika Viruses," *Infection, Genetics and Evolution* 93 (2021): 104967.

23. S. R. da Silva Neto, T. Tabosa Oliveira, I. V. Teixeira, et al., "Machine Learning and Deep Learning Techniques to Support Clinical Diagnosis of

29439981, 2026, 2, Downloaded from https://advanced.onlinelibrary.wiley.com/doi/10.1002/aidi.202500049 by Universidade Estadual Paulista, Wiley Online Library on [28/09/2026]. See the Terms and Conditions (https://onlinelibrary.wiley.com/terms-and-conditions) on Wiley Online Library for rules of use; OA articles are governed by the applicable Creative Commons License

Arboviral Diseases: A Systematic Review," *PLoS Neglected Tropical Diseases* 16, no. 1 (2022): e0010061.

24. A. Zeba, A. Rajalingam, K. Sekar, and A. Ganjiwale, "Machine Learning-Based Gene Expression Biomarkers to Distinguish Zika and Dengue Virus Infections: Implications for Diagnosis," *VirusDisease* 35, no. 3 (2024): 446–461.

25. E. W. Brown, M. W. Glasscott, K. Conley, et al., "ACEstat: A Diy Guide to Unlocking the Potential of Integrated Circuit Potentiostats for Open-Source Electrochemical Analysis," *Analytical Chemistry* 94, no. 12 (2022): 4906–4912.

26. L. Stratmann, B. Heery, and B. Coffey, "EmStat Pico: Embedded Electrochemistry with a Miniaturized, Software-Enabled Potentiostat System on Module," *Analog Devices* (2019), TA21437 - 9/19.

27. R. Salahandish, F. Haghayegh, G. Ayala-Charca, et al., "Bi-ECDAQ: An Electrochemical Dual-Immuno-Biosensor Accompanied by a Customized Bi-Potentiostat for Clinical Detection of SARS-CoV-2 Nucleocapsid Proteins," *Biosensors and Bioelectronics* 203 (2022): 114018.

28. J. I. de Oliveira Filho and K. N. Salama, *"Live dDemonstration: KAUSTat—a cCompact rReconfigurable eElectrochemical sStation,"* in 2022 IEEE Sensors, IEEE (2022), pp. 1–1.

29. P. Lopin and K. V. Lopin, "PSoC-Stat: A Single Chip Open Source Potentiostat Based on a Programmable System on a Chip," *PloS One* 13, no. 7 (2018): e0201353.

30. D. Beduk, J. I. de Oliveira Filho, T. Beduk, et al., "'All In One'SARS-CoV-2 Variant Recognition Platform: Machine Learning-Enabled Point of Care Diagnostics," *Biosensors and Bioelectronics: X* 10 (2022): 100105.

31. T. Beduk, D. Beduk, J. I. de Oliveira Filho, et al., "Rapid Point-of-Care COVID-19 Diagnosis with a Gold-Nanoarchitecture-Assisted Laser-Scribed Graphene Biosensor," *Analytical Chemistry* 93, no. 24 (2021): 8585–8594.

32. I. Anshori, et al., "Design of Smartphone-Controlled Low-Cost Potentiostat for Cyclic Voltammetry Analysis Based on ESP32 Microcontroller," *Sensing and Bio-Sensing Research* 36 (2022): 100490.

33. S. C.-H. Lee and P. J. Burke, "NanoStat: An Open Source, Fully Wireless Potentiostat," *Electrochimica Acta* 422 (2022): 140481.

34. K. A. Bautista, E. Madsen, S. D. Riegle, and J. C. Linnes, "HELPStat: A Handheld, EIS-Enabled, Low-Cost, and Portable Potentiostat," *ACS Electrochemistry* 1, no. 3 (2025): 386–394.

35. P. Baldi and P. J. Sadowski, "Understanding Dropout," *Advances in Neural Information Processing Systems* 26 (2013): 2814–2822.

36. N. Srivastava, G. Hinton, A. Krizhevsky, I. Sutskever, and R. Salakhutdinov, "Dropout: A Simple Way to Prevent Neural Networks from Overfitting," *The Journal of Machine Learning Research* 15, no. 1 (2014): 1929–1958.

37. M. Chua, D. Kim, J. Choi, et al., "Tackling Prediction Uncertainty in Machine Learning for Healthcare," *Nature Biomedical Engineering* 7, no. 6 (2023): 711–718.

38. J. D. S. Oliveira and E. J. Guidelli, "Multitherapeutic Nanoplatform Based on Scintillating Anthracene, Silver@ Anthracene, and Gold@ Anthracene Nanoparticles for Combined Radiation and Photodynamic Cancer Therapies," *Materials Science and Engineering: C* 126 (2021): 112122.

39. B. B. Junior, M. R. Batistuti, A. S. Pereira, E. M. de Sousa Russo, and M. Mulato, "Electrochemical Aptasensor for NS1 Detection: Towards a Fast Dengue Biosensor," *Talanta* 233 (2021): 122527.

Supporting Information

Additional supporting information can be found online in the Supporting Information section.

29439981, 2026, 2, Downloaded from https://advanced.onlinelibrary.wiley.com/doi/10.1002/aidi.202500049 by Universidade Estadual Paulista, Wiley Online Library on [28/09/2026]. See the Terms and Conditions (https://onlinelibrary.wiley.com/terms-and-conditions) on Wiley Online Library for rules of use; OA articles are governed by the applicable Creative Commons License